Contents lists available at ScienceDirect

Arabian Journal of Chemistry

journal homepage: www.ksu.edu.sa

Original article

Fabrication of boron nitride/copper oxide@multi-walled carbon nanotubes composites for enhancing heat transfer and photothermal conversion of phase change materials

Weifang Han [a,*], Deyi Liu [a], Guoliang Wang [a], Suliang Li [b], En You [b], Zhengfeng Jia [a], Yuchao Li [a,*]

[a] School of Materials Science and Engineering, Liaocheng University, Liaocheng 252059, China
[b] Construction Eighth Engineering Division, Zhejiang Construction Engineering Co., Ltd. of China, Hangzhou 311215, China

ARTICLE INFO

Keywords:
Phase change composite
Thermal conductivity
Thermal management
Photothermal conversion
Thermal energy storage

ABSTRACT

To realize the efficient storage and conversion of solar energy by phase change materials (PCMs), low photothermal conversion efficiency and poor heat transfer performance remain great challenges. Herein, polyethylene glycol (PEG)-based composite PCMs with excellent photothermal conversion performance and exceptional thermal management capability were obtained by using boron nitride/copper oxide@multi-walled carbon nanotubes (BN/CuO@MWCNTs) as the thermal conductive and photothermal conversion enhancement fillers. The results indicate that owing to the bridging effect, the introduction of CuO and MWCNTs on the BN surface can construct additional heat transfer paths, resulting in a high thermal conductivity of up to 2.35 W/(m·K) for the as-prepared PEG/BN/CuO@MWCNTs composite, which is about 9-folds enhancement than pristine PEG. Simultaneously, the supercooling degree of PEG in PEG/BN/CuO@MWCNTs is effectively suppressed due to the synergistic nucleation effect of BN, CuO and MWCNTs. Additionally, the PEG/BN/CuO@MWCNTs composites not only exhibit a high latent-heat capacity of 154.5 J/g and a high photothermal conversion efficiency of 92.2 %, but also show favorable shape stability and durable reliability. This work offers a workable solution for the synergistic enhancement of photothermal conversion and thermal management, which can effectively promote the practical application in solar energy conversion and storage.

1. Introduction

The collection and utilization of solar energy play vital in the development and application of renewable energy (Liu et al., 2024; Xu et al., 2023; Li et al., 2024). Solar photothermal energy-storage technology based on phase change materials (PCMs) is considered to be a promising way to utilize solar energy (Pan et al., 2023; Albdour et al., 2022; Zheng et al., 2022). Nevertheless, the low thermal conductivity (TC) and inferior light absorption capacity of conventional PCMs (such as paraffin wax, fatty acids, hydrates, sugar alcohols and salt hydrate.) severely limit their photothermal conversion efficiency (η) and endothermic/exothermic rate (Zhang et al., 2024; Jiang et al., 2024; Huang et al., 2024). This long-standing bottleneck has emerged as a critical challenge for their applications, gradually evolving into a prominent scientific issue in this field (Liu et al., 2021). Therefore, simultaneously improving the TC and η of PCMs to enhance the comprehensive efficiency of solar energy utilization is still a very challenging bottleneck problem.

Introducing highly thermally conductive fillers (e.g., ceramics (Chen et al., 2022), metals (Zhu et al., 2024); metallic oxide (Chen et al., 2022); MXene (Chen et al., 2023) and carbon-based materials (Yang et al., 2023) into PCMs to prepare composite PCMs has been regarded as an effective approach to solve the low TC problem. Among various candidate fillers, hexagonal boron nitride (h-BN) holds significant potential for development due to extraordinary TC, outstanding electrical insulation performance and superior stability, particularly for applications under extreme conditions such as high temperatures, strong acids and alkaline environments (Wang et al., 2024). Unfortunately, the TC enhancement is far from satisfactory due to poor compatibility and unexpected aggregation of BN filler (Zhou et al., 2024). Although surface modification of BN filler could reduce the interfacial thermal resistance (ITR) in the interfacial regions, the obtained TC enhancement effect did not meet expectations due to inadequate functionalization

* Corresponding authors.
E-mail addresses: hanweifang@lcu.edu.cn (W. Han), liyuchao@lcu.edu.cn (Y. Li).

https://doi.org/10.1016/j.arabjc.2024.105997
Received 18 July 2024; Accepted 17 September 2024
Available online 18 September 2024
1878-5352/© 2024 The Authors. Published by Elsevier B.V. on behalf of King Saud University. This is an open access article under the CC BY-NC-ND license (http://creativecommons.org/licenses/by-nc-nd/4.0/).

Nomenclature

PCMs	phase change materials
PEG	polyethylene glycol
BN	boron nitride
CuO	copper oxide
MWCNTs	multi-walled carbon nanotubes
PW	paraffin wax
GO	graphene oxide
PVA	poly(vinyl alcohol)
Fe_3O_4	ferroferric oxide
H_3BO_3	Boric acid
$C_3H_6N_6$	melamine
$CuSO_4$	copper sulfate
$NH_3{\cdot}H_2O$	aqueous ammonia
EP	epoxy resin
NaOH	sodium hydroxide
BNNS	boron nitride nanosheets
PVP	polyvinylpyrrolidone
TC	thermal conductivity
η	photothermal conversion efficiency
ITR	interfacial thermal resistance
δ	TC improvement per 1 wt% filler loading
T_m	melting temperature
T_c	crystallization temperature
ΔH_m	melting enthalpy
ΔH_c	crystallization enthalpy
ΔT	supercooling degree

(Jiang et al., 2020). In addition, adding a large amount of BN filler can greatly increase the TC value of composite PCMs, but their energy storage density will be significantly reduced. Numerous studies have demonstrated that metal nanoparticles (Cu (Wang et al., 2020); Ag (Ma et al., 2023) and Zn (Xu et al., 2023) and carbon-based materials (MWCNTs (Shi et al., 2023) and GO (Bashir et al., 2023) loaded on the BN surface can act as functional bridges that create additional contacts between adjacent BN, facilitating the formation of 3D heat flowpath. For instance, Shi et al. reported EP/BNNS@AgNPs composites in which AgNPs functioned as a "bridge" to connect the neighbouring BNNS, ultimately achieving significant enhancement of heat transfer performance (Chen et al., 2019). The TC of the EP/BNNS@Ag composite with the addition of 20 wt% BNNS@AgNPs was 1.13 W/(m·K), which was 1.14 times higher than that of the EP/BNNS composite without AgNPs. These findings have provided a series of effective strategies for the development of PCM-based composites with an enhanced TC for accelerating the endothermic/exothermic rate.

In practical applications, besides the requirement for further enhancement of TC, it is also essential to consider the η of PCMs. The introduction of light-absorbing media (such as carbon-based materials (Yang et al., 2024); precious metal NPs (Zhang et al., 2022) and metallic oxide (Wang et al., 2024) and so on) with excellent photothermal conversion capabilities into PCMs been considered as a potentially effective method to enhance the η of the PCMs for solar energy utilization. Among them, 1D carbon nanotubes (CNTs) not only have high TC, but also strong light absorption ability, and can convert light energy into heat through lattice vibration (Sun et al., 2022). For example, Kong et al. prepared MWCNT/MF/PW composites using multi-walled CNTs (MWCNTs), melamine foam (MF) and paraffin wax (PW) as the photothermal conversion material, supporting skeleton and PCMs, respectively (Dai et al., 2024). The obtained composite has a high η (85.16 %). Previous researches have provided evidence that there is a strong correlation between the structure of CNTs and their photothermal properties. For example, 3D CNTs networks, CNTs arrays and CNTs aerogels can reduce the reflection of light and achieve efficient light absorption (Chen et al., 2023; Zhou et al., 2022). Copper oxide (CuO) is a typical p-type semiconductor nanomaterial with a narrow band gap of 1.2–1.9 eV (Pang et al., 2024). Due to its small size and surface effect, good light absorption and excellent TC, it has a wide range of applications in the fields of solar absorbers, optoelectronic devices and catalysis (Yang et al., 2022). Adjusting the size, morphology or structure of CuO could provide another feasible ways for regulating their spectral absorption capabilities, which can also avoid the complex process of loading metal nanoparticles (Zhang et al., 2020). However, CuO has poor stability and are prone to aggregation after prolonged light irradiation in the PCMs matrix, which weakens the light absorption performance and leads to poor η. The photothermal hybrid material obtained by loading CuO and CNTs onto the surface of BN can combine the advantages of each material and enhance the photothermal effect through synergistic and complementary effects (Yang et al., 2022). The loading of CuO and CNTs on the BN surface effectively prevents their agglomeration and increases the surface roughness, which not only increases the area of absorbed light, but also attenuates the reflection of light, thus contributing to the enhancement of light trapping. In addition, due to the bridging effect, the introduction of CNTs can construct additional heat transfer paths to further improve the phonon transmission density (Deng et al., 2023). CuO anchored on BN reduce the ITR between BN and CNTs, suppress phonon scattering and accelerate phonon transport (Ma et al., 2023). Thus, it is expected that the introduction of hybrid materials constructed from BN, CNTs, and CuO into PCMs will not only improve the η well, but also enhance the heat transfer performance.

Guided by this design concept, we proposed a synergistic strategy to enhance the heat transfer performance and photothermal conversion capability of PEG-based composite PCMs using BN/CuO@MWCNTs hybrid. The as-obtained PEG/BN/CuO@MWCNTs composite PCMs exhibit a high TC of 2.35 W/(m·K) at 10 wt% filler loading, about 904 % higher than that of pure PEG, which may be attributed to the construction of continuous thermal conduction paths by the combination of BN, CuO and MWCNTs. The CuO and MWCNTs endow the composite PCMs with outstanding photothermal conversion performance, and the corresponding η is increased to 92.2 %. Meanwhile, the PEG/BN/CuO@MWCNTs composite PCMs display favorable shape-stability, low supercooling degree and high thermal storage performance, suggesting their potential to be used as thermal storage materials for the design of the next generation of solar energy harvesting systems.

2. Experimental section

2.1. Materials

Boric acid (H_3BO_3, purity ≥ 99.5 %), melamine ($C_3H_6N_6$, purity ≥ 99.0 %), copper sulfate ($CuSO_4$, purity ≥ 99.0 %), polyethylene glycol (PEG, Mn = 6000 w, purity ≥ 99.0 %), aqueous ammonia ($NH_3{\cdot}H_2O$, AR, 28–30 %), sodium hydroxide (NaOH, purity ≥ 96.0 %) and polyvinylpyrrolidone (PVP, M_n = 10 000 w, purity ≥ 99.0 %) were purchased from Sigma-Aldrich. Multi-walled carbon nanotubes (MWCNTs, outer diameter: 5–10 nm, length: 10–30 μm, purity >95 %) were acquired from Jiangsu Cnano Technology Co., Ltd.

2.2. Preparation of BN microrods

The preparation of BN microrods was based on our previous report with minor modifications (Han et al., 2023). In detail, 6.18 g H_3BO_3 and 6.31 g $C_3N_6H_6$ were dissolved in 150 mL deionized (DI) water and stirred at 90 °C for 4 h. Subsequently, $H_3BO_3{\cdot}2C_3N_6H_6$ (B·2M) precursors were obtained by washing, filtering, and drying. Finally, the

precursors were heated under N_2 atmosphere at 1100 °C with a temperate ramp of 5 °C/min for 2 h to obtain the targeted BN microrods.

2.3. Fabrication of BN/CuO hybrids

Firstly, 6.18 g H_3BO_3, 6.31 g $C_3N_6H_6$, and predetermined amounts of $CuSO_4$ were introduced into 150 mL DI water, then $NH_3{\cdot}H_2O$ was dropwise added until until pH = 10. The blue mixture was vigorously stirred at 90 °C for 4 h. After that, the resulting mixture was washed, filtered, and dried to gain M·2B/$Cu(OH)_2$ precursors. Finally, the precursors were calcined in N_2 atmosphere at 1100 °C for 2 h to obtain BN/CuO hybrids. The raw material amounts used to prepare BN/CuO hybrids were detailed in **Table S1**.

2.4. Preparation of BN/CuO@MWCNTs composites

A schematic illustrating the fabrication of the BN/CuO@MWCNTs composites is demonstrated in Fig. 1. 6.18 g H_3BO_3, 6.31 g $C_3N_6H_6$, 3.20 g $CuSO_4$ and 1.0 g PVP were dissolved in 150 mL DI water at 90 °C, and predetermined amounts of MWCNTs were then introduced with continuous stirring for an additional 4 h. Subsequently, $NH_3{\cdot}H_2O$ was slowly added until pH = 10. After that, the M·2B/$Cu(OH)_2$@MWCNTs precursors were gained after washing and drying. Eventually, the precursors were heated under N_2 at 1100 °C for 2 h to obtain BN/CuO@MWCNTs composite. The raw material amounts used to prepare BN/CuO@MWCNTs composites with different contents of MWCNTs were detailed in **Table S2**.

2.5. Preparation of PEG/BN/CuO@MWCNTs composite PCMs

PEG/BN/CuO@MWCNTs with different amounts of BN/CuO@MWCNTs were synthesized via a melt-blending process. Firstly, 10 g of dehydrated PEG powder was stirred at 80 °C to form a homogeneous solution. Then, predetermined amounts of BN/CuO@MWCNTs were slowly added into the PEG solution. After stirring at 80 °C for 4 h, the mixed slurries were poured into a Teflon-coated mold. Finally, the PEG/BN/CuO@MWCNTs composite PCMs were obtained by cooling at room temperature.

2.6. Characterization

The morphological and compositional evolution were observed by scanning electron microscopy-energy dispersive X-ray spectroscopy (SEM-EDX, Zeiss MERLIN Compact, Germany). The structural characteristics were investigated through a Fourier Transform Infrared spectrometer (FTIR, Bruker Tensor-27, Germany) and an X-ray diffraction diffractometer (XRD, Rigaku, SmartLab, Japan). The elemental composition and surface chemical state were measured by an X-ray photoelectron spectroscopy (XPS, Thermo Fisher Scientific K-Alpha, USA). Accordingly, the differential scanning calorimetry (DSC, TA Instruments Q20, USA) analysis was employed to measure the endothermic/exothermic curves. The ability of absorption light was measured by an ultraviolet–visible–near–infrared diffuse reflectometer (UV–vis–NIR, Shimadzu UV-3600i Plus, Japan) equipped with an integrating sphere. The TC of composites was measured by a thermal constant analyzer (Netzsch LFA 457, Germany). Thermal transfer performance was photographed with an IR camera (Fotric 626C, China). Solar simulator with a temperature recorder (Yili Technology Co., Ltd., China) for continuous and uninterrupted surface temperature.

3. Results and discussion

Fig. 2**a-c** show the SEM images of the BN, BN/CuO hybrid and BN/CuO@MWCNTs composite. The as-synthesized BN displays a one-dimensional rod-like structure with a smooth surface, a length of 5–10 μm and a diameter of 2–4 μm (Fig. 2**a**). The growth of CuO on the surface of BN can be optimized by controlling the additive molar ratio of H_3BO_3 to $CuSO_4$ ($R_{B/Cu}$), and the corresponding morphologies are provided in Fig. 2**b** and **Fig. S1**. When the $R_{B/Cu}$ is 5.0, a mass of CuO (10–50 nm) is evenly anchored on the surface of BN microrods with almost no aggregation or stacking (Fig. 2**b**). In addition, CuO can bridge neighbouring BN microrods, which is beneficial for reducing the ITR between adjacent BN (Wang et al., 2020). The elemental composition and distribution of the BN/CuO hybrid are further characterized by XPS spectrum and elemental mapping analysis, and the results are shown in **Fig S2** and **Fig S3**. The analyses reveal that the BN/CuO hybrid contains B, N, Cu, and O elements, which are uniformly distributed across the entire area. Overall, the following studies are conducted using BN/CuO hybrid prepared with $R_{B/Cu}$ of 5. The microstructures of the BN/CuO@MWCNTs composites with different MWCNTs contents were observed by SEM (Fig. 2**c** and **Fig. S4**). The BN/CuO@MWCNTs composites are composed of rod-like structured BN, tubular MWCNTs and granular CuO. When an appropriate amount of MWCNTs is added (Fig. 2**c**), the surface of the BN/CuO@MWCNTs composite has dense and uniform MWCNTs, which are tightly intertwined to form a core–shell structure. The entangled and well-dispersed MWCNTs form an interlaced network, which effectively fill the gaps between the BN/CuO hybrids. Additionally, related results of element mapping analysis of BN/CuO@MWCNTs composite are displayed in Fig. 2**d-h**. B, N, C, Cu, and O elements are homogeneously distributed on the surface of microrods, indicating that the BN/CuO@MWCNTs composite is successfully prepared.

The chemical and phase structures of the samples were investigated by FTIR spectroscopy and XRD patterns (Fig. 3). The FTIR spectrum of BN microrod, BN/CuO hybrid and BN/CuO@MWCNTs composite are shown in Fig. 3**a**. BN microrod shows two intense peaks at 1380 and 803

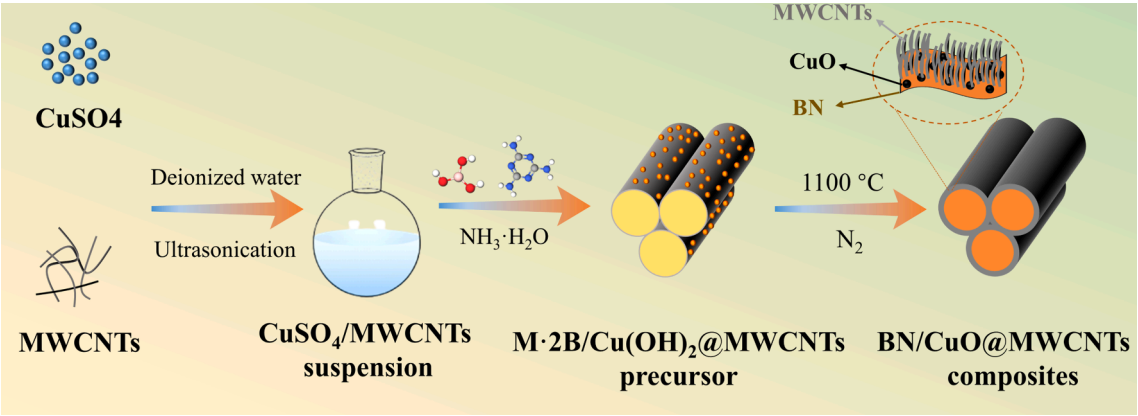

Fig. 1. Schematic of the preparation procedure of BN/CuO@MWCNTs composites.

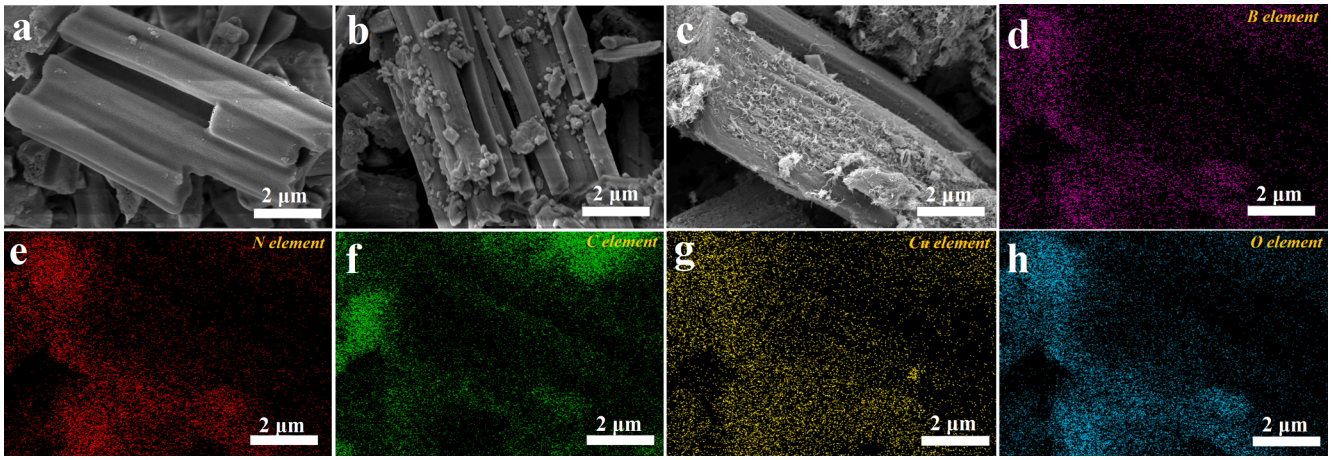

Fig. 2. SEM images of (a) BN, (b) BN/CuO hybrid, (c) BN/CuO@MWCNTs composite, and corresponding elemental mapping images of BN/CuO@MWCNTs composite: (d) B, (e) N, (f) C, (g) Cu and (h) O elements.

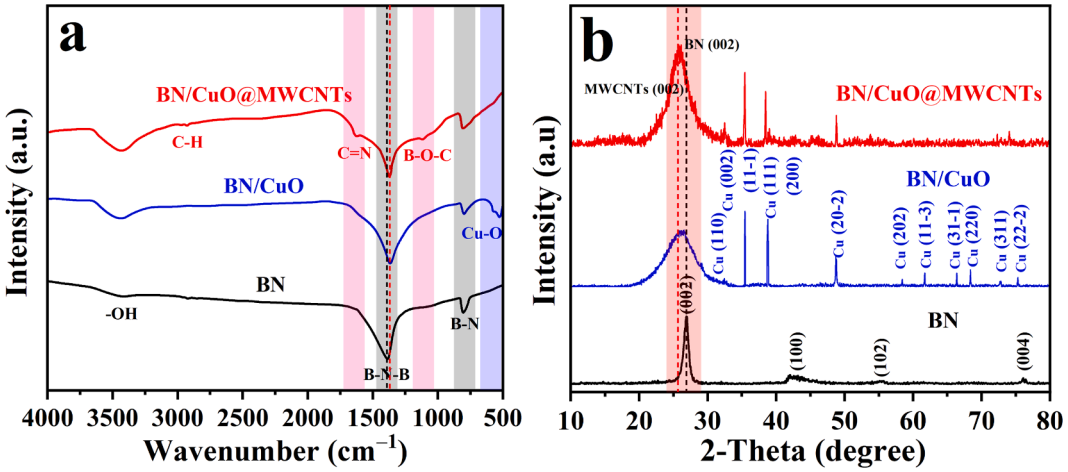

Fig. 3. (a) FTIR spectrum and (b) XRD patterns of BN microrod, BN/CuO hybrid and BN/CuO@MWCNTs composite.

cm^{-1}, which are caused by the stretching and bending vibrations of B-N, respectively (Han et al., 2022). In addition, an additional characteristic signal located at ~3423 cm^{-1} corresponds to the —OH group, reflecting the high activity of the synthesised BN microrod (Han et al., 2024). When CuO NPs are introduced, a typical absorption peak appears at 525 cm^{-1}, which is associated with Cu—O (Pang et al., 2024). Moreover, B—N—B vibration in the BN/CuO hybrid moves in a low-wavenumber direction, implying a weak interaction between BN and CuO. For the BN/CuO@MWCNTs composite, the peaks observed at 1112.1 and 1268 cm^{-1} are assigned to the B—O—C and C—N, indicating the formation of covalent bonds between BN and MWCNTs (Bashir et al., 2023).

The XRD patterns of the BN microrod, BN/CuO hybrid and BN/CuO@MWCNTs composite are shown in Fig. 3**b**. BN sample possesses four reflections at 2θ of 26.9°, 42.3°, 55.6°, and 76.2°, which is associated with the (002), (100), (102), and (004) crystal planes of h-BN structure (JCPDS card no. 34-0421), respectively (Han et al., 2023). For BN/CuO hybrid and BN/CuO@MWCNTs composite, the peaks at 2θ = 32.5°, 35.4°, 38.7°, 48.7°, 58.4°, 61.7°, 66.4°, 68.3°, 72.7° and 75.3°can be indexed to the (110), (11−1), (111), (20−2), (202), (11−3), (31−1), (220), (311) and (22−2) planes of the monoclinic crystalline phase of CuO (JCPDS card no. 48-1548) (**Fig. S5**) (Yan and Li, 2023). Compared with the BN/CuO hybrid, the BN/CuO@MWCNTs composite exhibits a broad peak at 25.8°, which may be due to the (002) plane of BN overlapping with that of MWCNTs. In addition, some of the characteristic peaks of CuO disappear in BN/CuO@MWCNTs composite, presumably because CuO is covered by MWCNTs.

The elemental composition and valence states of the BN/CuO@MWCNTs composite were determined by XPS spectra (Fig. 4). Five characteristic peaks are detected in the XPS survey spectrum (Fig. 4**a**), corresponding to B, C, N, O and Cu signals, respectively. Fig. 4**b-f** show the high-resolution B 1s, N 1s, Cu 2p, C 1s and O 1s XPS energy spectrum, respectively. The B1s spectrum (Fig. 4**b**) could be fitted with three peaks at 191.0, 192.4 and 193.9 eV, representing the B—N, B—O and B—C bonds, respectively (Zare and Moradi, 2022). As shown in Fig. 4**c**, the N 1s peak can be fitted into two peaks, which result from the N—B (399.7 eV) and N—C bonds (398.5 eV). For Cu 2p spectra (Fig. 4**d**), two characteristic peaks at 934.4 and 954.4 eV correspond to the binding energies of Cu 2p$_{3/2}$ and Cu 2p$_{1/2}$, respectively, and the difference in their binding energies is 20 eV, implying the formation of Cu^{2+} species. Moreover, two strong satellite peaks are observed, further manifesting the presence of Cu^{2+} species (Maity et al., 2022). The deconvoluted C 1s spectra can be fitted into three peaks (Fig. 4**e**). The main peak at 284.7 eV is associated with the C—C/C═C bands. The peaks at the binding energy of 285.1 and 285.7 eV correspond to the C—N and C—O—B bonds (Sekar et al., 2021). As depicted in Fig. 4**f**, the O 1s spectra can be divided into three fitted peaks at 531.6, 532.7 and 533.9 eV, which are related to Cu—O—Cu, C—O—B and Cu—O—B bonds, respectively (Zare and Moradi, 2022; Li et al., 2023). Taken together, the abovementioned results suggest that BN, CuO and MWCNTs are successfully combined to form BN/CuO@MWCNTs

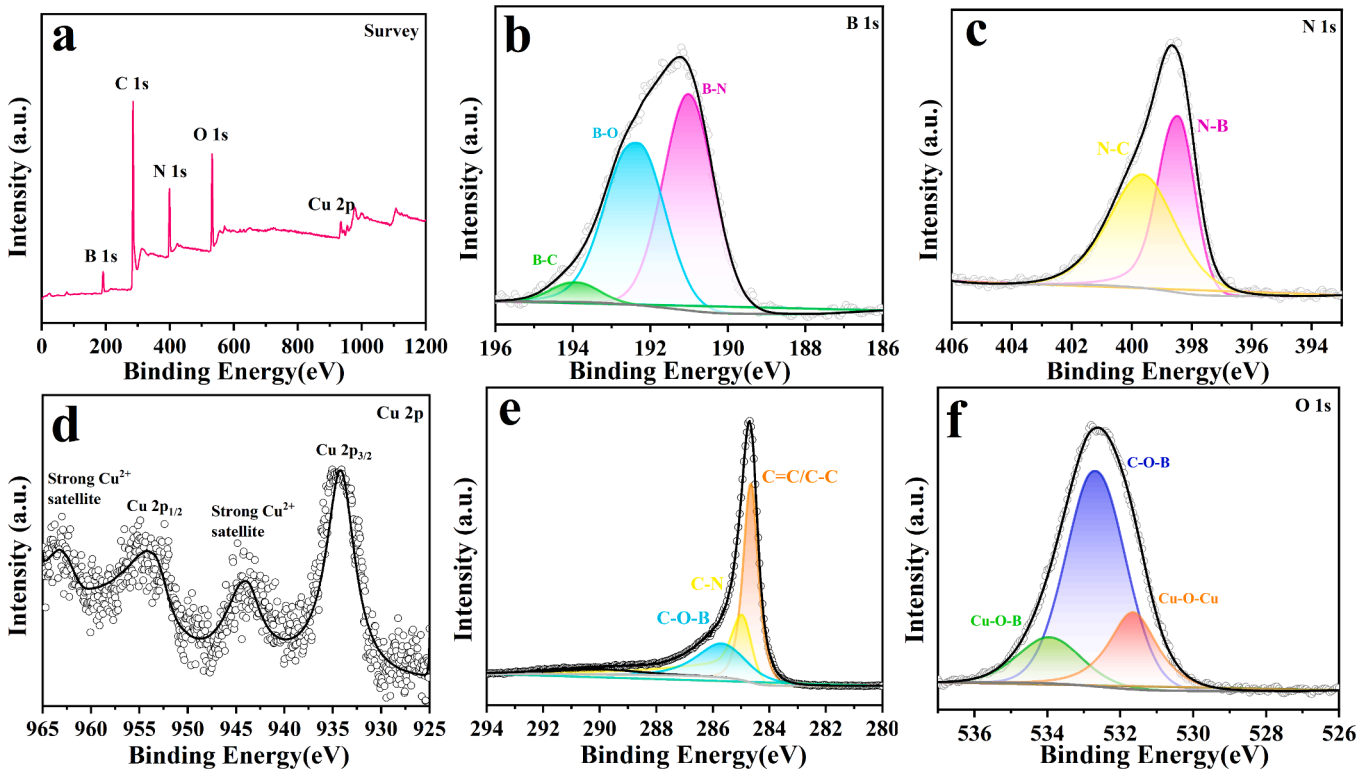

Fig. 4. (a) Survey XPS spectrum, the high-resolution spectrum of (b) B 1s, (c) N 1s, (d) Cu 2p (e) C 1s and (f) O 1s of BN/CuO@MWCNTs composite.

composite.

In general, the TC value is one of the important indexes for evaluating the endothermic/exothermic rate of composite PCMs. Fig. 5**a** shows the effect of the mass fraction of filler on the TC values of PEG-based composites. Pure PEG is a poor thermal conductor with a low TC of 0.26 W/(m·K), which is mainly due to the severe phonon scattering of the molecular chain (Guo et al., 2020). For the PEG/BN composite, the TC values are slightly enhanced with the increase of BN addition. By contrast, the TC values of PEG/BN/CuO composites are dramatically higher than PEG/BN composites. The reason is that CuO can act as a "solder joint" to ensure good contact with the BN to create thermally conductive paths in the composite, which significantly

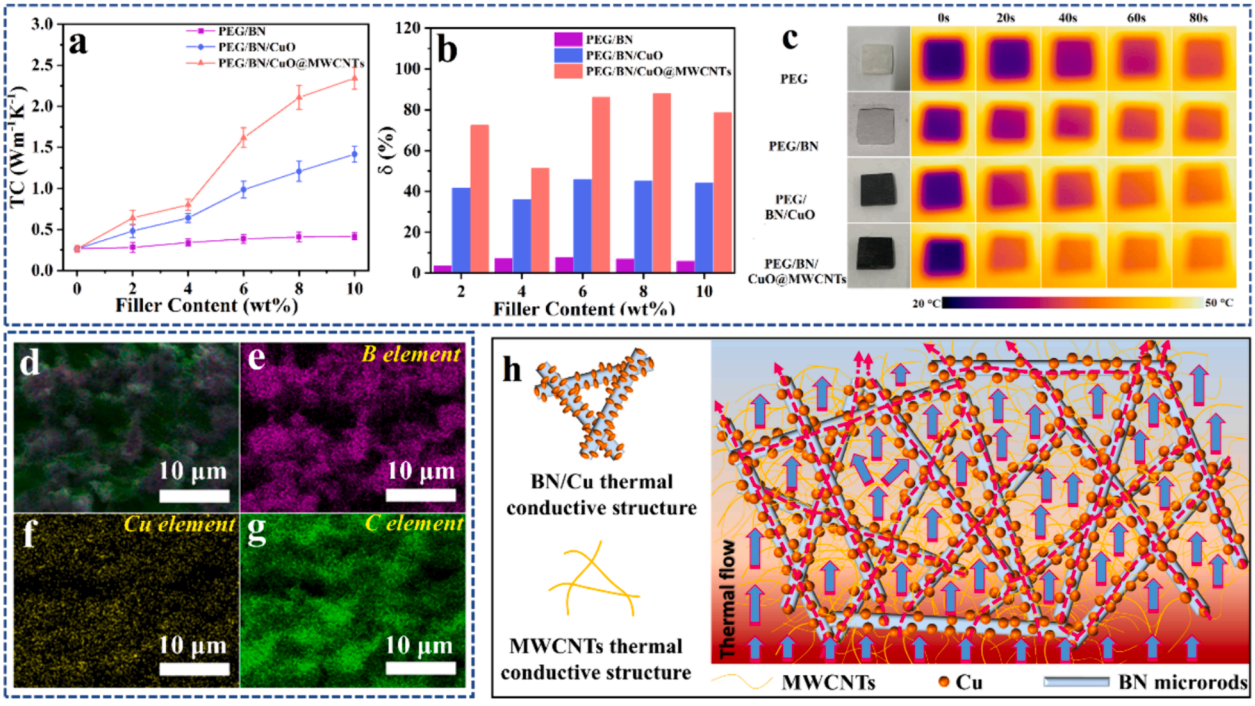

Fig. 5. (a) TC and (b) TC enhancement (c) infrared thermal images of PEG/BN, PEG/BN/CuO and PEG/BN/CuO@MWCNTs composites, (d) cross-sectional SEM image and (e-g) corresponding element distribution, (h) the possible thermal conduction manners of PEG/BN/CuO@MWCNTs composite.

reduces the ITR (Wang et al., 2020; Xu et al., 2023). Moreover, when BN/CuO@MWCNTs are introduced, the TC values of PEG/BN/CuO@MWCNTs composites show a significant upward trend. Overall, the TC values present the result that PEG/BN/CuO@MWCNTs > PEG/BN/CuO > PEG/BN at the same filler addition. For instance, the TC value of PEG/BN/CuO@MWCNTs composite achieves 2.35 W/(m·K) with 10 wt% filler contents, about 9.0, 5.6 and 1.7 times higher than that of pure PEG, PEG/BN and PEG/BN/CuO. Additionally, the factor (δ) is introduced to further evaluate the TC improvement per 1 wt% filler loading on the composites by using the following Eq. (1) (Han et al., 2023).

$$\delta = \frac{TC_{COM} - TC_{PEG}}{100_{wf} TC_{PEG}} \times 100\% \quad (1)$$

where w_f is the mass fraction of filler; TC_{PEG} and TC_{COM} are the TC values of pure PEG and PEG-based composite PCMs, respectively. As demonstrated in Fig. 5**b**, the δ of PEG/BN/CuO@MWCNTs reaches the maximum value of 88 % at only 8 wt% filler loading, which is much higher than that of PEG/BN and PEG/BN/CuO. This is attributed to the formation of a dense thermally conductive BN/CuO@MWCNTs network in the PEG matrix.

To investigate the thermal response rate, the samples with the same size are placed on a graphite heating plate at 50 °C for 80 s, and the evolutions of the surface temperatures are monitored using an infrared camera (Fig. 5**c and Fig. S6**). As shown in Fig. 5**c**, the infrared heat images of PEG/BN/CuO@MWCNTs present the fastest color change from blue to orange compared to the pure PEG, PEG/BN, PEG/BN/CuO samples during the heating process, suggesting that the PEG/BN/CuO@MWCNTs has rapid thermal response rate, which could facilitate thermal energy transfer.

The cross-sectional SEM image, element distribution and the possible TC enhancement mechanism of the PEG/BN/CuO@MWCNTs composite are shown in Fig. 5**d-h**. Firstly, CuO adhered to BN surface can reduce the ITR between BN and MWCNTs, which accelerates phonon transport and suppresses phonon scattering (Xu et al., 2023). Secondly, due to the bridging effect, the introduction of MWCNTs can construct additional heat transfer paths to further improve the phonon transmission density (Xia et al., 2020). Therefore, the heat flow can be quickly transferred to the interior of the PEG/BN/CuO@MWCNTs composite PCMs through the thermally conductive network, which strongly supports the improvement of the thermal storage rate.

The phase-change enthalpy and phase transition temperature are critical parameters for evaluating the performance of PCMs. Thus, the endothermic/exothermic curves of samples were investigated by DSC (Fig. 6**ab**). The detailed thermophysical data obtained from the DSC curves, such as the melting/crystallization temperature (T_m/T_c) and the melting/crystallization enthalpy ($\Delta H_m/\Delta H_c$), are listed in **Table S3**. The PEG/BN, PEG/BN/CuO and PEG/BN/CuO@MWCNTs composite PCMs display similar DSC curves with pure PEG, suggesting the absence of chemical reactions between the substrate and fillers. Compared to the pure PEG, the ΔH_m and ΔH_c of composite PCMs slightly decrease, primarily because BN, CuO, and MWCNTs in the composite do not undergo a phase transition process. In addition, the T_m of PEG, PEG/BN, PEG/BN/CuO and PEG/BN/CuO@MWCNTs in the heating process are 58.6, 58.1, 57.5 and 56.4 °C, respectively. The lowest T_m of the PEG/BN/CuO@MWCNTs composite PCMs may be due to the efficient heat pathways formed by BN/CuO@MWCNTs inside the composite PCMs, which promotes the thermal movement of PEG molecular chains. In the cooling process, The T_c of the PEG/BN/CuO@MWCNTs is 43.8 °C, 5.4, 3.8, and 2.1 °C higher than that of PEG, PEG/BN and PEG/BN/CuO, respectively, which can be attributed to the fact that the BN/CuO@MWCNTs with a high specific surface area provides a large number of nucleation sites for PEG and reduces nucleation activation energy (Lei et al., 2019).

Evaluation of the supercooling degree (ΔT) of PCMs is important for practical applications, which can be obtained through the formula $\Delta T = T_m - T_c$. The ΔT of PEG, PEG/BN, PEG/BN/CuO and PEG/BN/CuO@MWCNTs are 20.2, 18.1, 15.8 and 12.6 °C, respectively (Fig. 6**c**). The PEG/BN/CuO@MWCNTs composite has the lowest ΔT, because the BN/CuO@MWCNTs as nucleation agent promotes PEG crystallization. On the one hand, the BN/CuO@MWCNT with a high specific surface area and large roughness provides the heterogeneous nucleation sites for

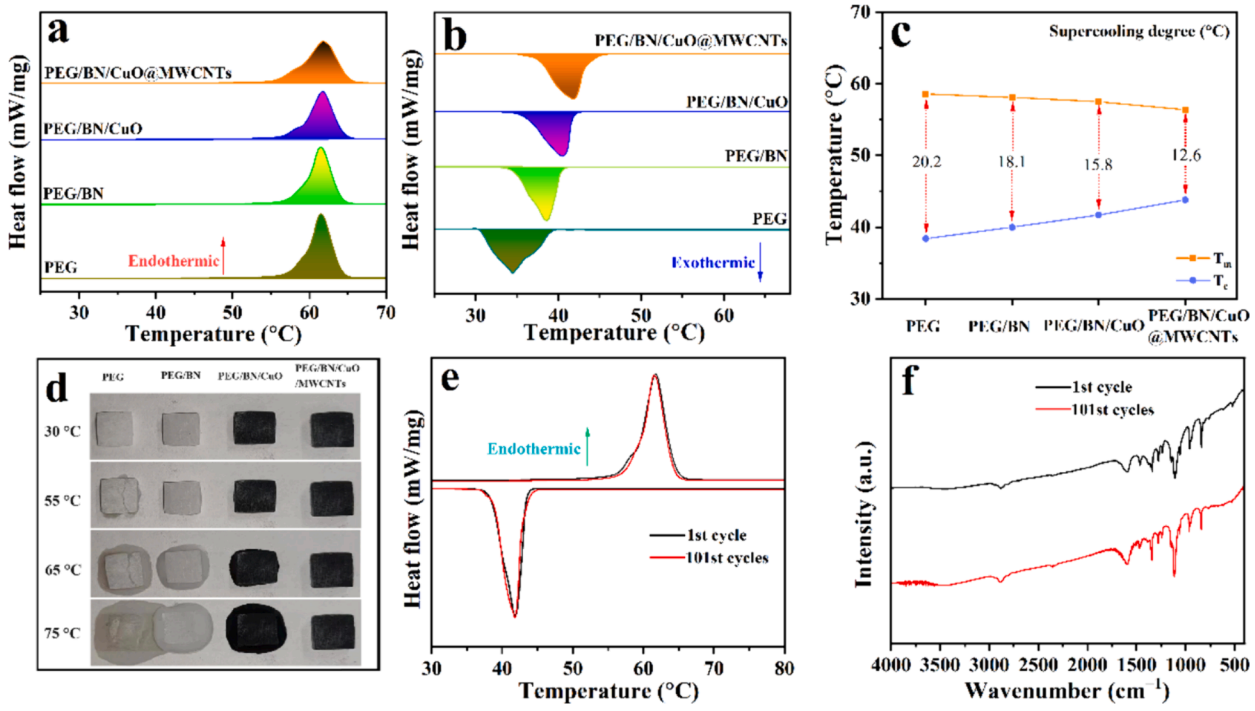

Fig. 6. (a, b) DSC curves, (c) supercooling degree and (d) shape-stability of PEG, PEG/BN, PEG/BN/CuO and PEG/BN/CuO@MWCNTs composites, (e) DSC curves (f) and FTIR spectra of BN/CuO@MWCNTs composite before and after 100 thermal cycles.

PEG crystal growth (**Fig. S7**) (Li et al., 2023). On the other hand, BN/CuO@MWCNT has good surface wettability with PEG due to the presence of oxygen-containing groups, which reduces the nucleation activation energy of PEG (Chen et al., 2023).

In practical applications, the leakage of PCMs decreases the energy storage density and contaminates the contact equipment. To examine the shape-stability, the samples are heated from 30 to 75 °C, and the process is captured with a digital camera (Fig. 6**d**). At 30 °C, all samples are in a solid-state and maintain their original circular shape. The pure PEG melts and displays obvious liquid leakage as the temperature rises to 55 °C, while slight leakage is also observed in the PEG/BN. The PEG/BN/CuO and PEG/BN/CuO@MWCNTs composite PCMs exhibit excellent shape-stability with no signs of liquid leakage. With further heating up to 65 °C, the leakage of the pure PEG and PEG/BN samples becomes more visible, whereas the PEG/BN/CuO begins to showcase slight leakage. Furthermore, the PEG/BN/CuO@MWCNTs composite still could retain its original shape at 75 °C (~16 °C above the melting point of pure PEG) without significant PEG leakage, whereas the other samples show significant melt leakage, indicating that it has excellent shape-stability. The PEG/BN/CuO@MWCNTs composite PCMs have a denser inner interconnected network due to the attachment of MWCNTs to the BN/CuO surface, which can effectively encapsulate PEG (Deng et al., 2023). Meanwhile, the hydrogen bonds between —OH on the PEG and O electronegative atom on the surface of BN/CuO@MWCNTs restrict the movement of the PEG molecular chain. This enables PEG/BN/CuO@MWCNTs composite PCMs to remain shape-stable even at a melting temperature much higher than that of pure PEG.

Furthermore, the stable reversibility of the PEG/BN/CuO@MWCNTs composite PCMs is explored by the DSC cycling test and FTIR spectra (Fig. 6**e-f**). As displayed in Fig. 6**e**, the ΔH_m and ΔH_c of composite PCMs remain constant after 101 heating cycles. After thermal cycling, the peak shapes and wavenumbers in the FTIR spectra are also unchanged (Fig. 6**f**). These results demonstrate that PEG/BN/CuO@MWCNTs composite PCMs have excellent reliability and long-term stability.

To realize the energy harvesting, conversion and storage of composite PCMs with the same surface area and weight by photo-thermal routes, an experimental setup was designed to conduct the light-thermal conversion test (Fig. 7**a**). The temperature variations were recorded as a function of time using a thermocouple recorder under 100 mW/cm^2 simulated solar irradiation (Fig. 7**b**). Under simulated solar irradiation, the saturation surface temperatures of PEG and PEG/BN reach 39 and 43 °C at 300 s without inflection points or platforms, indicating that the phase transition behaviour did not occur, which can be explained by the poor light absorption properties of PEG and BN. For PEG/BN/CuO and PEG/BN/CuO@MWCNTs composites, the surface temperatures rapidly increase in the initial stage and then reach a stable plateau, suggesting that solar energy is converted into thermal energy and stored through phase transition. After the completion of the phase change process, the secondary warming process occurs until the saturated temperature is achieved. Impressively, the saturated temperature of PEG/BN/CuO@MWCNTs is 84 °C, which is superior to that of the PEG/BN/CuO (68 °C), showcasing outstanding light-absorbing ability and photothermal conversion performance. Upon the turn-off light source irradiation, the PEG/BN/CuO@MWCNTs composite shows a significant liquid–solid phase change plateau that lasts for more than 100 s, which represents the heat-releasing process. These results reveal that PEG/BN/CuO@MWCNTs composite PCMs can rapidly transform the absorbed light into thermal energy, and spontaneously store thermal energy through a phase transition, thereby remarkably increasing the efficiency of solar thermal utilization.

To further verify the superiority of PEG/BN/CuO@MWCNTs composite PCMs, the η is estimated using the following Eq. (2) (Liu et al., 2024):

$$\eta = \frac{m\Delta H_m}{ps(t_2 - t_1)} \tag{2}$$

where m, ΔH_m and s are respectively the weight (g), fusion enthalpy (J) and surface area (cm^2) of the samples. P is the power of the simulated solar irradiation (mW/cm^2). t_1 and t_2 are the onset and end times of light-driven phase transition taking place in the samples, respectively, which are obtained by the tangential method (Fig. 7**b**) (Chen et al., 2023). The data required for calculating the η of the sample is listed in **Table S4**. Based on **Eq. (2)**, the η values of the PEG/BN/CuO and PEG/BN/CuO@MWCNTs are approximately 75.8 % and 92.2 %, respectively. The improvement in the photothermal storage efficiency of PEG/BN/CuO@MWCNTs is attributed to the introduction of BN/CuO@MWCNTs to enhance the absorption enhancement in the UV–Vis–NIR regions (**Fig. S8**). In addition, the heat transfer and photothermal conversion properties of PEG/BN/CuO@MWCNTs were compared to those of other PEG-based PCMs, as shown in **Table S5**. Compared with other studies, the comprehensive performance of PEG/BN/CuO@MWCNTs demonstrates highlight advantages.

4. Conclusion

In summary, PEG/BN/CuO@MWCNTs composite PCMs for photothermal conversion and storage were fabricated by the combination of BN with CuO and MWCNTs via the high-temperature solid-state method and incorporating BN/CuO@MWCNTs into PEG. The limitations in terms of low η and TC have been effectively overcome through the rational design of the structure. In particular, the PEG/BN/CuO@MWCNTs composite PCMs possess a remarkable TC of 2.35 W/

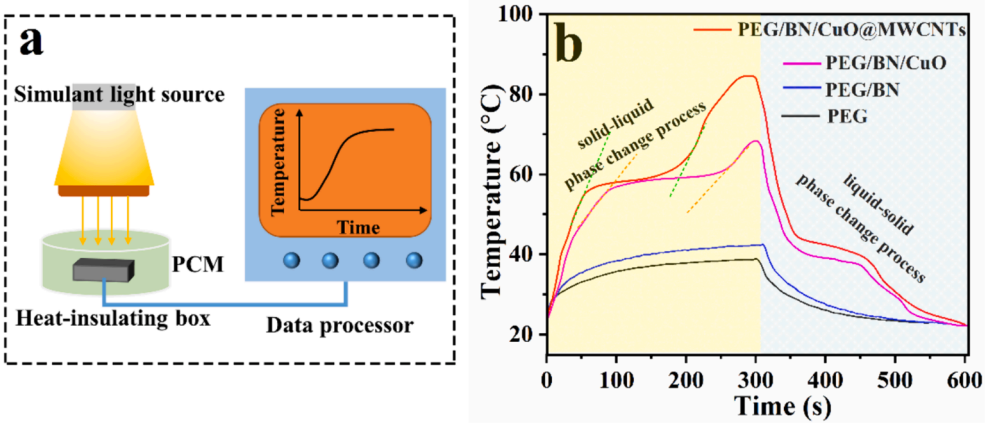

Fig. 7. (a) The diagram of setup for light-thermal conversion experiment, (b) time–temperature curves of PEG, PEG/BN, PEG/BN/CuO and PEG/BN/CuO@MWCNTs composites.

(m·K) with 10 wt% filler additions, which is about 803.8 % higher than the pure PEG. Meanwhile, the composite PCMs not only display high latent heat of 154.5 J/g and a high η of 92.2 %, but also show outstanding shape-stability after heating at 50 °C and maintain a high thermal cycle stability after thermally cycled for 100 times. Meanwhile, due to the synergetic nucleating effect of BN, CuO and MWCNTs, the supercooling of PEG/BN/CuO@MWCNTs was effectively suppressed from 20.2 °C to 12.6 °C. Consequently, PEG/BN/CuO@MWCNTs composite PCMs with excellent comprehensive performance have great potential in the collection, conversion and storage of solar energy.

CRediT authorship contribution statement

Weifang Han: Writing – original draft, Methodology, Investigation, Funding acquisition, Formal analysis, Data curation. **Deyi Liu:** Methodology, Investigation, Formal analysis, Data curation. **Guoliang Wang:** Methodology, Investigation. **Suliang Li:** Formal analysis. **En You:** Investigation, Conceptualization. **Zhengfeng Jia:** Writing – review & editing. **Yuchao Li:** Writing – review & editing, Funding acquisition.

Declaration of competing interest

The authors declare that they have no known competing financial interests or personal relationships that could have appeared to influence the work reported in this paper.

Acknowledgments

The authors thank the Natural Science Foundation of Shandong Province (ZR2020QE044, ZR2020ME133 and ZR2020ME035), National Natural Science Foundation of China (52177020), Research Fund for the Doctoral Program of Liaocheng University (318051938) and Student Innovation Training Program of Liaocheng University (CXCY2023013, CXCY007 and CXCY008) for funding and supporting this work.

Appendix A. Supplementary data

Supplementary data to this article can be found online at https://doi.org/10.1016/j.arabjc.2024.105997.

References

Albdour, S.A., Haddad, Z., Sharaf, O.Z., Alazzam, A., Abu-Nada, E., 2022. Micro/nano-encapsulated phase-change materials (ePCMs) for solar photothermal absorption and storage: Fundamentals, recent advances, and future directions. Prog. Energy Combust. Sci. 93, 101037.

Bashir, A., Maqbool, M., Lv, R., Usman, A., Aftab, W., Niu, H., Kang, L., Bai, S., 2023. Engineering of interfacial interactions among BN and CNT hybrid towards higher heat conduction within TPU composites. Compos. Part A 167, 107428.

Bashir, A., Maqbool, M., Usman, A., Lv, R., Niu, H., Kang, L., Ashraf, Z., Bai, S., 2023. Enhancing thermal conductivity and mechanical strength of TPU composites through modulating o-PDA-BN/rGO heterointerface networks. Compos. Part A 173, 107676.

Chen, Y., Chen, J., Hao, Z., Selim, M.S., Yu, J., Chen, X., 2023. Polyvinylpyrrolidone-bridged MXene skeleton constructed by photothermal assisted sacrificial template method for phase change materials with form stability and photothermal conversion. Chem. Eng. J. 463, 142375.

Chen, C., Xue, Y., Li, Z., Wen, Y., Li, X., Wu, F., Li, X., Shi, D., Xue, Z., Xie, X., 2019. Construction of 3D boron nitride nanosheets/silver networks in epoxy-based composites with high thermal conductivity via in-situ sintering of silver nanoparticles. Chem. Eng. J. 369, 1150–1160.

Chen, C., Gong, L., Jiang, W., Chen, Z., Chen, W., Du, X., Zhou, H., Huang, Z., Zhou, H., 2023. Light-trapping carbon nanotube forests in glass fibre-reinforced thermoplastic prepregs for efficient laser-assisted automated fibre placement. Compos. Sci. Technol. 235, 109971.

Chen, S., Liu, H., Wang, X., 2022. Pomegranate-like phase-change microcapsules based on multichambered TiO2 shell engulfing multiple n-docosane cores for enhancing heat transfer and leakage prevention. J. Energy Storage 51, 104406.

Chen, Q., Wang, H., Gao, H., Wang, X., Ma, B., 2022. Effects of porous silicon carbide supports prepared from pyrolyzed precursors on the thermal conductivity and energy storage properties of paraffin-based composite phase change materials. J. Energy Storage 56, 106046.

Dai, H., Yuan, J., Kong, X., Zhao, C., 2024. Shape-memory phase change material enhanced by MWCNT for solar photothermal conversion. Sol. Energy Mater. Sol. Cells 269, 112756.

Deng, J., Kou, Y., Liu, H., Yang, M., Sun, K., Joshi, R., Shi, Q., 2023. Melamine foam/CNT/graphene hybrid aerogel-based phase change composites with high latent heat capacity for solar/eectrothermal conversion. ACS Appl. Energy Mater. 6, 7457–7467.

Guo, Y., Ruan, K., Shi, X., Yang, X., Gu, J., 2020. Factors affecting thermal conductivities of the polymers and polymer composites: A review. Compos. Sci. Technol. 193, 108134.

Han, W., Chu, X., Li, Y., Xu, Z., Li, W., Fu, P., Li, Y., Zhang, X., Jia, Z., Zhang, X., 2022. Anchoring modified polystyrene to boron nitride nanosheets as highly thermal conductive composites for heat dissipation. Polym. Compos. 43, 1844–1851.

Han, W., Zhang, X., Chen, M., Chu, X., Li, W., Fu, P., Jia, Z., Li, Y., 2023. Construction of multilayered boron nitride nanosheets for improving optical performance and stability of rhodamine B. Dyes Pigm. 215, 111244.

Han, W., Yuan, C., Chen, M., Ma, W., Zhuang, F., Li, W., Zhang, X., 2023. Anchoring carbon nanotubes to boron nitride microrods for enhancing the thermal conductivity of polystyrene. Ceram. Int. 49, 2140–2148.

Han, W., Liu, D., Zhou, Y., Zhang, H., Xing, A., Fu, P., Jia, Z., Lin, Y., Li, Y., Li, W., 2024. Growth of polyaniline nanowire arrays on boron nitride microrods enables high-efficient thermal transport. Polym. Compos. 45, 7790–7800.

Huang, Y., Luo, W., Chen, W., Hu, X., Zhu, G., Ma, Y., Jiang, X., Li, Q., 2024. Self-healing, adaptive and shape memory polymer-based thermal interface phase change materials via boron ester cross-linking. Chem. Eng. J. 496, 153789.

Jiang, F., Cui, X., Song, N., Shi, L., Ding, P., 2020. Synergistic effect of functionalized graphene/boron nitride on the thermal conductivity of polystyrene composites. Compos. Commun. 20, 100350.

Jiang, Z., Liu, X., He, F., Li, Y., Chen, Z., Li, X., Wang, P., He, G., Yang, W., 2024. Shape-stabilized phase change materials for thermal energy storage and heat dissipation. Colloids Surf., A 688, 133559.

Lei, C., Wu, K., Wu, L., Liu, W., Du, R., Chen, F., Fu, Q., 2019. Phase change material with anisotropically high thermal conductivity and excellent shape stability due to its robust cellulose/BNNSs skeleton. J. Mater. Chem. A 7, 19364–19373.

Li, H., Li, Y., Wang, C., Han, C., Xu, K., Zhang, Z., Zhong, Q., Shi, K., Xu, Z., Yang, S., Li, S., He, H., Song, H., Zhang, S., 2023. Improved degradation of iohexol using electro-enhanced activation of persulfate by a Cu_xO-loaded carbon felt with carbon nanotubes as an interlayer. Sep. Purif. Technol. 312, 123336.

Li, J., Long, Y., Cao, X., Sun, H., Jiao, R., Zhu, Z., Liang, W., Li, A., 2024. Recent advances and perspectives in solar photothermal conversion and storage systems: A review. Adv. Colloid Interface Sci. 325, 103118.

Li, Q., Tan, Y., Lin, C., Ning, Y., Yu, L., Cao, Z., Sun, L., Zeng, J., 2023. Preparation and properties of erythritol/exfoliated graphite nanoplatelets @ polyaniline microencapsulated phase change materials with improved photothermal conversion efficiency. J. Energy Storage 72, 108553.

Liu, Y., Liu, Y., Chen, W., Hu, X., He, Y., Ma, Y., Xie, Y., Luo, W., Luo, L., Jiang, L., Jiang, X., Li, Q., 2024. Polyethylene glycol/melamine foam composite phase change materials modified by CdS/Ag exhibits high photothermal conversion performance. Desalination 585, 117783.

Liu, H., Qian, Z., Liao, G., Wang, X., 2021. Integration of magnetic phase-change microcapsules with black phosphorus nanosheets for efficient harvest of solar photothermal energy. ACS Appl. Energy Mater. 4, 13248–13262.

Liu, C., Wang, L., Li, Y., Diao, X., Dong, C., Li, A., Chen, X., 2024. Fe_3O_4/carbon-decorated graphene boosts photothermal conversion and storage of phase change materials. J. Colloid Interface Sci. 657, 590–597.

Ma, Y., Zou, M., Chen, W., Luo, W., Hu, X., Xiao, S., Luo, L., Jiang, X., Li, Q., 2023. A structured phase change material integrated by MXene/AgNWs modified dual-network and polyethylene glycol for energy storage and thermal management. Appl. Energy 349, 121658.

Maity, C.K., De, S., Acharya, S., Siddiki, S.H., Sahoo, S., Verma, K., Thakur, V.K., Nayak, G.C., 2022. Copper oxide stabilized oxy-functionalized boron nitride-carbon nanotube nanohybrid: An ultra-stable electrode for flexible asymmetric supercapacitor device in ionic electrolyte. J. Energy Storage 56, 105928.

Pan, C., Li, X., Fan, G., Yang, H., Long, Y., Wu, F., 2023. Low-cost and highly thermally conductive silver modified mica-paraffin multifunctional composite phase change materials for photo-thermal conversion and electrical insulation. Arabian J. Chem. 16, 105310.

Pang, H., Li, G., Cheng, L., He, C., Wang, X., Zhang, X., 2024. 3D flower-like CuO@PEG composite phase change materials with photo response for applications in energy conversion and storage. J. Energy Storage 82, 110537.

Sekar, S., Gawas, P., Bhat, S.V., Nutalapati, V., 2021. Highly fluorescent 2D-BCNO sheets based chemical sensor for selective detection of the explosive dunnite and 4-nitrophenol in aqueous medium. Environ. Sci.: Nano 8, 2908–2919.

Shi, W., Song, N., Huang, Y., Wang, W., He, C., Zhao, W., Zhao, C., 2023. Enhanced thermal conductive and moisturizing hydrogels by constructing 3D networks of BN-OH and CNT-OH in alignment for burn therapy. Mater. Des. 233, 112239.

Sun, Z., Shi, T., Wang, Y., Li, J., Liu, H., Wang, X., 2022. Hierarchical microencapsulation of phase change material with carbon-nanotubes/polydopamine/silica shell for synergistic enhancement of solar photothermal conversion and storage. Sol. Energy Mater. Sol. Cells 236, 111539.

Wang, Y., Wu, W., Drummer, D., Liu, C., Shen, W., Tomiak, F., Schneider, K., Liu, X., Chen, Q., 2020. Highly thermally conductive polybenzoxazine composites based on boron nitride flakes deposited with copper particles. Mater. Des. 191, 108698.

Wang, Y., Du, K., Liu, B., He, C., Zhao, B., Xiao, Z., 2024. Design and characterization of novel flexible phase change composite materials as protective liners for the cartridge case. Colloids Surf., A 684, 133254.

Wang, L., Zhou, M., Fu, H., 2024. An in-situ growth Fe_3O_4 and polyaniline on carbon cloth encapsulated composite phase change materials with high thermal conductivity and photothermal energy conversion and storage. J. Energy Storage 78, 110090.
Xia, Y., Li, Q., Ji, R., Zhang, H., Xu, F., Huang, P., Zou, Y., Chu, H., Lin, X., Sun, L., 2020. Multielement synergetic effect of boron nitride and multiwalled carbon nanotubes for the fabrication of novel shape-stabilized phase-change composites with enhanced thermal conductivity. ACS Appl. Mater. Interfaces 12, 41398–41409.
Xu, Y., Xing, W., Liu, J., Song, C., 2023. Highly thermal conductive and rechargeable 3D liquid metal network-based phase change composite enabling photothermal pad. Compos. Commun. 43, 101719.
Xu, F., Zhu, J., Ye, P., Geng, H., Peng, J., Cui, Y., Bao, D., Lu, R., Shen, X., Zhu, H., Zhu, Y., Wang, H., 2023. Outstanding thermally conductive and anticorrosive polymer composite coating via a multifunctional epoxy curing agent zinc dimethacrylate. Chem. Eng. J. 473, 145163.
Yan, D., Li, M., 2023. Efficient solar thermal energy utilization and storage based on phase change materials stabilized by MOF@CuO composites. J. Energy Storage 73, 108885.
Yang, H., He, L., Liu, R., Ge, C., Ma, C., Zhang, X., 2022. Ultralight and flexible carbon-based phase change composites with high porosity for enhanced shape memory and photothermal conversion performance. Sol. Energy Mater. Sol. Cells 244, 111816.
Yang, H., Si, M., Guo, Y., Ge, C., He, L., Zhang, X., 2024. RHTC/HO-BNNS structure collaboratively improves thermal conductivity and photothermal conversion properties of phase change materials. Sol. Energy Mater. Sol. Cells 268, 112746.
Yang, P., Wu, B., Tong, X., Zeng, M., Wang, Q., Cheng, Z., 2023. Insight into heat transfer process of graphene aerogel composite phase change material. Energy 279, 128051.
Zare, M., Moradi, L., 2022. Preparation of hollow mesoporous boron nitride spheres with surface decorated by CuO: A bifunctional acid-base catalyst for the green synthesis of some heterocyclic [3,3,3] propellane derivatives in water media. Appl. Surf. Sci. 582, 152454.
Zhang, H., Wang, K., Wang, L., Xie, H., Yu, W., 2020. Mesoporous CuO with full spectrum absorption for photothermal conversion in direct absorption solar collectors. Sol. Energy 201, 628–637.
Zhang, J., Zeng, B., Li, D., Cui, Y., Wang, J., Duan, X., Chen, W., Liu, Q., Tang, B., 2022. Boron nitride-Au (Ag) loaded eggshell membrane with enhanced photothermal property. Colloids Surf., A 642, 128726.
Zhang, J., Zhang, J., Liu, D., Zeng, J., Ye, Z., Han, M., Zhang, S., Yao, Y., Sun, R., 2024. Collaborative electrospinning and ice-templating for sea urchin-inspired aerogel microsphere: Unraveling functional mechanisms in thermally conductive phase change composites. Compos. Sci. Technol. 250, 110538.
Zheng, Z., Shi, T., Liu, H., Wu, D., Wang, X., 2022. Polyimide/phosphorene hybrid aerogel-based composite phase change materials for high-efficient solar energy capture and photothermal conversion. Appl. Therm. Eng. 207, 118173.
Zhou, Z., Xia, H., Hu, J., Wang, L., 2024. Enhanced thermal energy storage of polyethylene glycol composite with high thermal conductive reaction-bonded BN aerogel. Compos. Commun. 49, 101965.
Zhou, S., Zhang, J., Wang, C., Wu, C., Zhang, X., Yang, Z., Zhang, X., 2022. Extremely black carbon nanotube materials with three-dimensional networks for highly efficient solar-driven vapor generation. Nanoscale 14, 17438–17446.
Zhu, G., Zou, M., Luo, W., Huang, Y., Chen, W., Hu, X., Jiang, X., Li, Q., 2024. A polyurethane solid–solid phase change material for flexible use in thermal management. Chem. Eng. J. 488, 150930.